Electronic Supplementary Materials

For https://doi.org/10.1631/jzus.A2500351

Sediment transport characteristics and siltation reduction method of high-pile wharves: a physical model and field observation study

Haojun YANG[1,2], Yangyang GAO[1,3], Lizhong WANG[1,3]

[1]*Ocean College, Zhejiang University, Hangzhou 310058, China*
[2]*School of Civil Engineering and Architecture, Taizhou Vocational & Technical College, Taizhou 318000, China*
[3]*Hainan Institute, Zhejiang University, Sanya 572025, China*

Section S1. Physical model experiment setup

The Froude scaling rule is applied to achieve hydrodynamic similarity since inertia and gravity forces are the predominant for the free surface and current. The similarity scale of the hydrodynamic is presented as follows (Zhang, 1998):

$$\lambda_u = \sqrt{\lambda_h} \tag{S1}$$

$$\lambda_n = \lambda_h^{\frac{2}{3}} \Big/ \sqrt{\lambda_l} \tag{S2}$$

$$\lambda_{t_1} = \frac{\lambda_l}{\lambda_u} = \frac{\lambda_l}{\sqrt{\lambda_h}} \tag{S3}$$

Since the study area is dominated by suspended sediment transport, the primary similarity criterion for sediment is settling velocity similarity, while the initiation velocity similarity should also be closely approximated. Additionally, the suspended sediment concentration in the tidal flow during experiments satisfies the similarity of sediment carrying capacity, as described below (Zhang, 1998):

$$\lambda_\omega = \frac{\lambda_u \lambda_h}{\lambda_l} \tag{S4}$$

$$\lambda_{u_c} = \lambda_u \tag{S5}$$

$$\lambda_S = \frac{\lambda_{\gamma_s}}{\lambda_{(\gamma_s-\gamma)/\gamma}} \tag{S6}$$

$$\lambda_{t_2} = \frac{\lambda_l \lambda_h \lambda_{\gamma_s'}}{\lambda_{qsb}} \tag{S7}$$

where γ_s is the unit weight of sediment, γ is the unit weight of water, γ_s' is the dry unit weight of sediment and the sediment transport rate scale λ_{qsb} can be estimated as follows:

$$\lambda_{q_{sb}} = \frac{\lambda_{\gamma_s}}{\lambda_{(\gamma_s-\gamma)/\gamma}} \lambda_h^{3/2} \tag{S8}$$

Combining Eq. (S6) and Eq. (S7), the sediment transport time scale λ_{t_2} can be estimated as:

$$\lambda_{t_2} = \frac{\lambda_l \lambda_{(\gamma_s-\gamma)/\gamma}}{\sqrt{\lambda_h}} \quad \text{(S9)}$$

The grain size distribution curve of the sediment in the study area is shown in Fig. 2(d), with a median particle size $d_{50} = 0.01\text{mm}$, the sediment settling velocity is calculated by $w_s = (\rho_s/\rho_w - 1)gd_{50}^2/18\upsilon$, where ρ_s is sand density and ρ_w is water density (Dallali and Armenio, 2015), and the sediment settling velocity $w_s = 8.99\times10^{-5}\text{m/s}$. The verification indicates that the paulownia wood powder with a median particle size of d_{50} = 0.03mm and a density of ρ_s = 1.18g/cm^3 better satisfy the similarity requirements for sediment settling and initiation. When d_{50} < 0.1 mm, the interaction between gravity and cohesive force must be considered (Singh et al., 2022), and Zhang Ruijin's formula is used to calculate the incipient velocity in the study area, presented as follows (Zhang, 1998):

$$U_c = \left(\frac{h}{d_{50}}\right)^{0.14}\left(17.6\frac{\rho_s-\rho_w}{\rho_w}d_{50} + 0.000000605\frac{10+h}{d_{50}^{\ 0.72}}\right)^{0.5} \quad \text{(S10)}$$

where U_c is the incipient velocity and h is the water depth. The incipient velocity in the study area is calculated by Equation (S10) as $U_{cm} = 0.944\text{m/s}$. To validate the incipient motion similarity of the model sand, a series of flume experiments were conducted at the Coastal Laboratory, Ocean College, Zhejiang University. The flume is 20m long, 0.5m wide, and 0.4m high. Both the sidewalls and the bottom are made of transparent glass to facilitate the observation of sediment transport. Before each experiment, the model sand (wood powder) was soaked in water for 12h and then evenly spread over the flume bed. The incipient motion velocity of the model sand was determined by visual observation. During the experiment, the flow velocity was gradually increased, and the sediment motion was recorded using a high-speed camera, as shown in Fig. S1. Following Dey and Raju (2002) and Beheshti and Ataie-Ashtiani (2008), the incipient condition was considered to be reached when all surface bed particles exhibited continuous movement for a certain period. The experimental results are summarized in Table S1. The measured incipient velocity of the model sand is 0.14m/s, and the corresponding incipient velocity scale is 6.74, which is close to the theoretical value of 7.07. This indicates that the selected model sand satisfies the incipient motion similarity requirement.

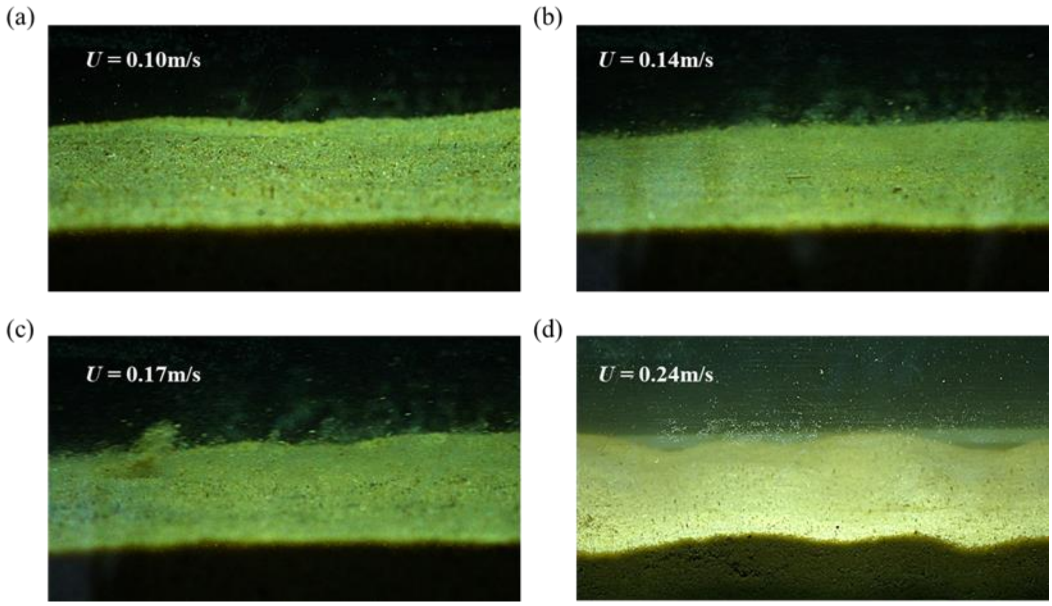

Fig. S1. Movement patterns of bedload under different flow velocities

Table S1. Model sand motion phenomenon

Flow velocity (m/s)	Phenomenon	Scale
0.10	Almost no particle initiation	9.44
0.14	A small amount of particle initiation	6.74
0.17	A large number of particle movement	5.55
0.24	Appearance of dunes and ripples	3.93

In the present study, the drag similarity is also be satisfied for the wharf pile group model. The drag force F_D of the pile group is expressed as $F_D = \rho C_D \left(\frac{A}{A_0}\right) A_0 \frac{u^2}{2}$, where A_0 is pile group envelope area, A is the sum of the projected areas of each single pile, and A/A_0 represents the pile group density. Then the drag ratio scale is:

$$\lambda_{F_D} = \frac{\left(\frac{A}{A_0}\sum C_D\right)_P}{\left(\frac{A}{A_0}\sum C_D\right)_m} \lambda_{A_0}\lambda_{u^2} = \frac{\left(\frac{A}{A_0}\sum C_D\right)_P}{\left(\frac{A}{A_0}\sum C_D\right)_m} \lambda_l \lambda_h^2 \quad \text{(S11)}$$

C_D is the drag coefficient. The drag scale ratio λ_{F_D} should be satisfied as follows:

$$\lambda_{F_D} = \lambda_\rho \lambda_g \lambda_l \lambda_h^2 = \lambda_l \lambda_h^2 \quad \text{(S12)}$$

where ρ is the water density, g is the gravity acceleration. Combining equations (S11) and (S12), the scale can be expressed as follows:

$$\left(\frac{A}{A_0}\sum C_D\right)_P = \left(\frac{A}{A_0}\sum C_D\right)_m \quad \text{(S13)}$$

The model pile is made of transparent plexiglass rods with a diameter of d = 8mm. Considering the prototype pile diameter is 1.2m and the spacing between the neighboring piles is 10m, resulting in a gap ratio of L/D = 8.3, the mutual interference effects on the drag coefficient could be negligible at this gap ratio (Aasland et al., 2022). The Reynolds number ($\mathrm{Re} = UD/\upsilon$) for the pile foundations in the study area is $\mathrm{Re} \sim 10^6$, the drag coefficient for the wharf prototype is taken as $(C_D)_p = 0.46$ (Ong et al., 2009).

Section S2. Physical model experiment validation

In this study, the physical model is validated against the field tide level and flow velocity data collected around the wharf during the spring tide in November 2021. The time-series comparisons of tide level, flow velocity, and flow direction at each measurement station between the field observations and the experimental results are presented in Figs. S2–S4, and the corresponding station locations are shown in Fig. 3a. The results indicate that an average deviation of ±7% in tidal levels with the field data, indicating the high accuracy in the predictions of tide level variations. Moreover, the comparison of flow velocity magnitude and direction (as shown in Fig. S3 and Fig. S4) indicates that the physical model effectively reproduces the variations in flow velocity magnitude and flow deflection during the tidal cycles. These validations confirm successful simulation of wharf hydrodynamics.

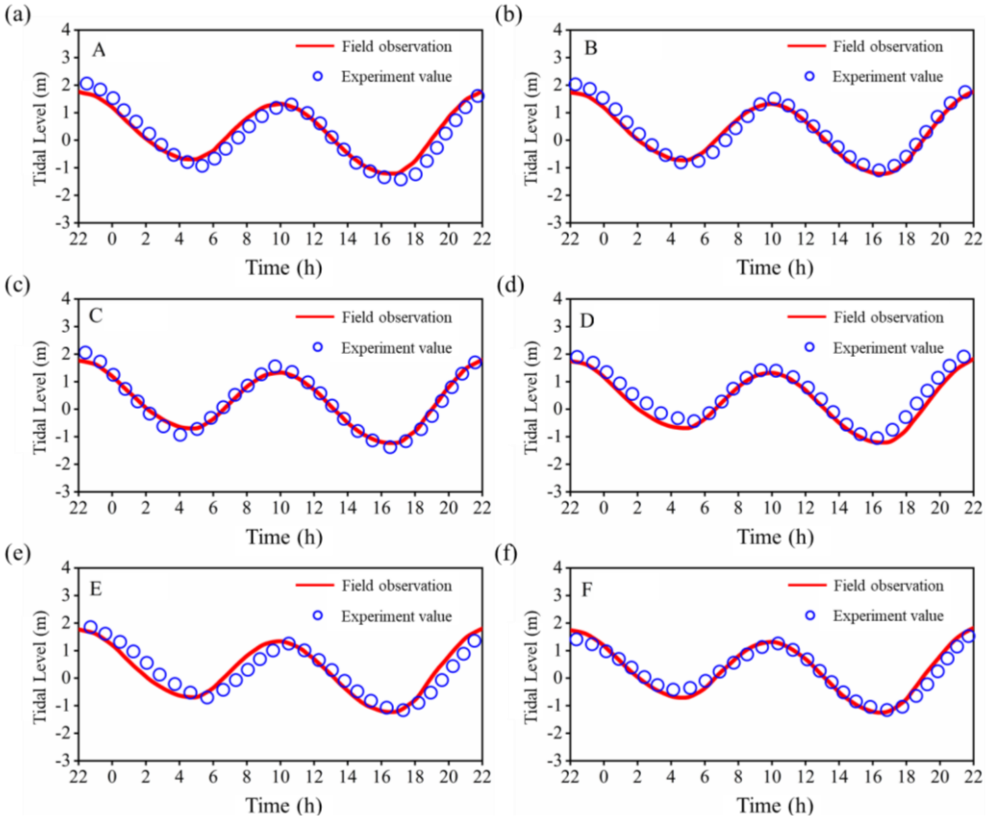

Fig. S2. Comparisons of tide level time series at each station between field observation and experimental data

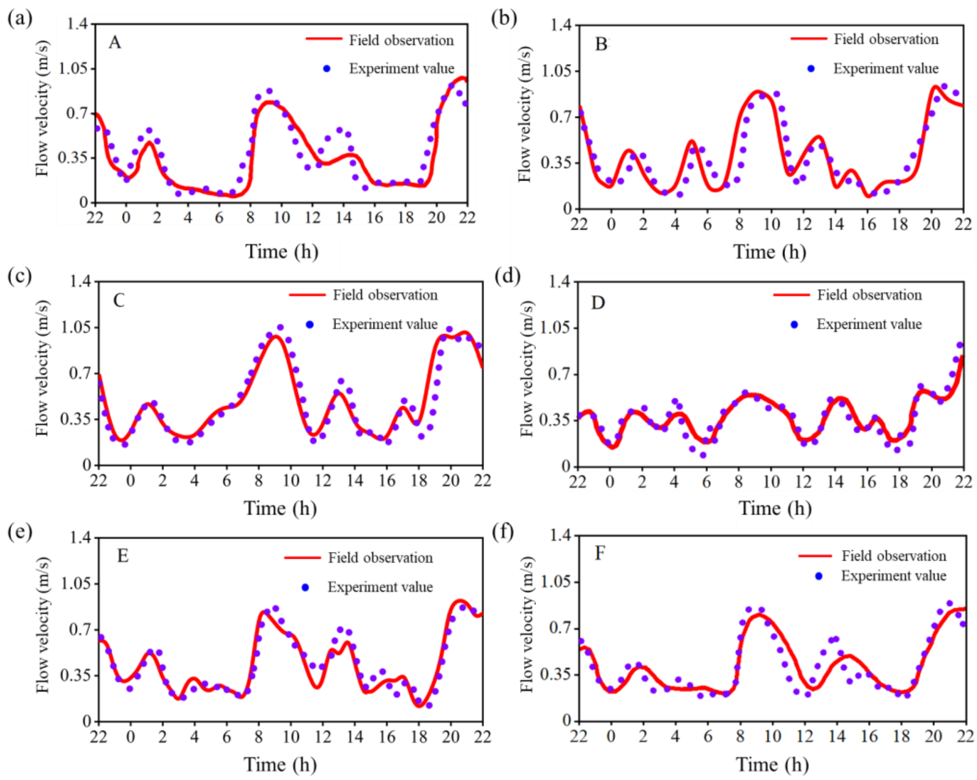

Fig. S3. Comparisons of flow velocity time series at each station between field observation and experimental data

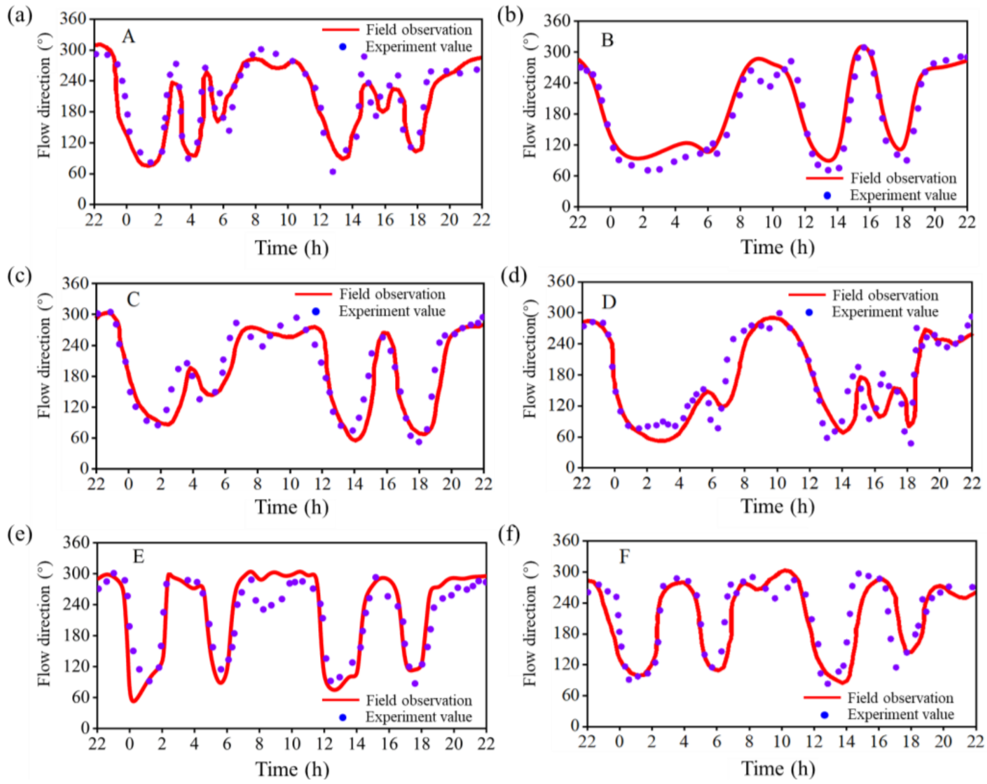

Fig. S4. Comparisons of flow direction time series at each station between field observation and experimental data

In the model, λ_{t_1} and λ_{t_2} represent the time scales of tidal cycle and sediment transport, respectively. λ_{t_2} is estimated using the empirical formulas in Eq. (S8) and requires additional calibration with field data to ensure accuracy. This study calibrates λ_{t_2} using sediment deposition height data behind 3# wharf from November 2020 to October 2022. Fig. S5 illustrates that the deposition heights obtained from the experimental results are closely to the field data for $\lambda_{t_2} = 156$.

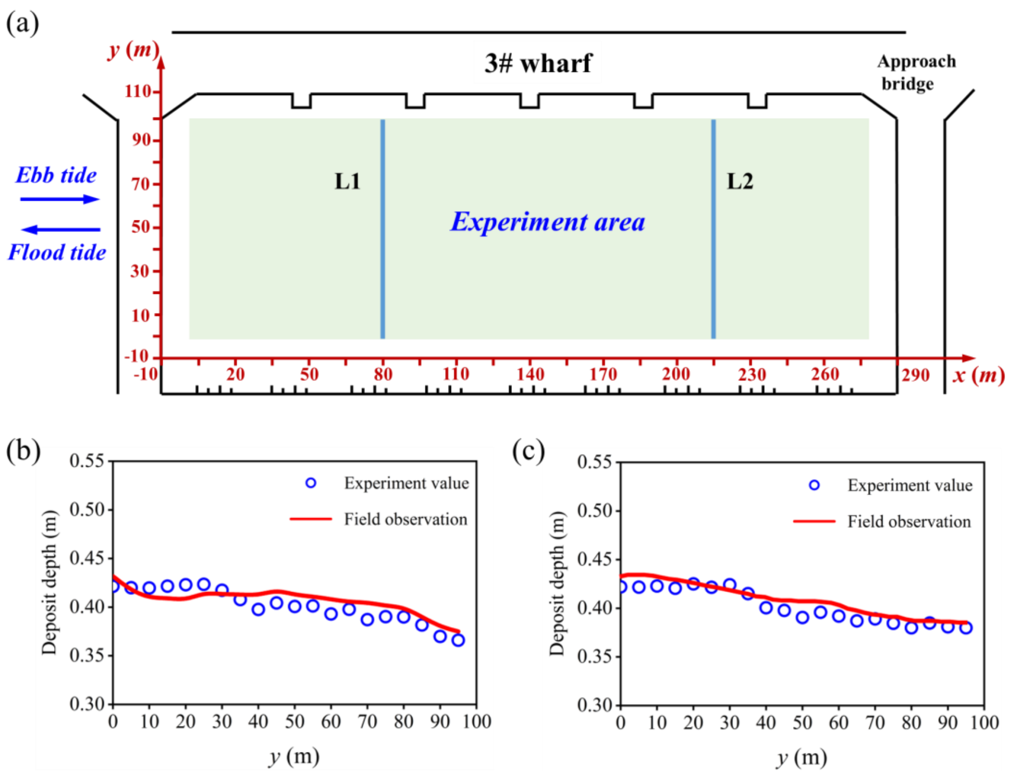

Fig. S5. Physical model sediment transport time scale correction; (a) experiment area and coordinate system establishment behind 3# wharf; (b) verification of deposit height in profile L1; (c) verification of deposit height in profile L2

Section S3. Limitations and Outlook

The present conclusions are derived from a site-specific setting at the Chuanshan Peninsula, characterized by fine cohesive sediment and an asymmetric tidal regime. The effectiveness of the groyne may vary with tidal asymmetry, sediment grain size and cohesion and topography settings. In addition, uncertainties remain due to the distorted depth scaling adopted in the physical model and the imperfect sediment similarity. The distorted scale may modify near-bed vertical velocity gradients and the distribution of bed shear stress, which can affect the magnitude and timing of sediment transport. The corrected scale ratios reported in Table 1 represent engineering compromises under material and facility constraints and may introduce uncertainty when extrapolating sediment transport intensity and transport time scale to prototype conditions. For very fine cohesive sediments, cohesion-related effects such as flocculation and consolidation are difficult to fully reproduce in the model, which may affect sediment initiation and settling processes. Future work will extend the analysis to additional sites and idealized configurations across a wider parameter range and validate the proposed mechanisms with targeted field observations and experiments.

Section S4. Velocity data processing and verification

During the data collection with the ADV, noise introduced by the field environment affects the data quality. To accurately analyze velocity variations and turbulence characteristics, it is necessary to filter out original velocity data with a correlation not exceeding 70% and reduce noise interference using the phase-space thresholding method (Goring and Nikora, 2002).

To verify the reliability of field ADV measurements and study near-bed flow structures, velocity sampling is conducted using a shipboard ADV near the tripod measurement point at 3# wharf along the water depth at high tide. The velocity profiles fit well with the rough wall log-law profiles (as shown in Fig. S6), ensuring the reliability of ADV velocity measurements and validating the reasonableness of the calculated friction velocity u_τ.

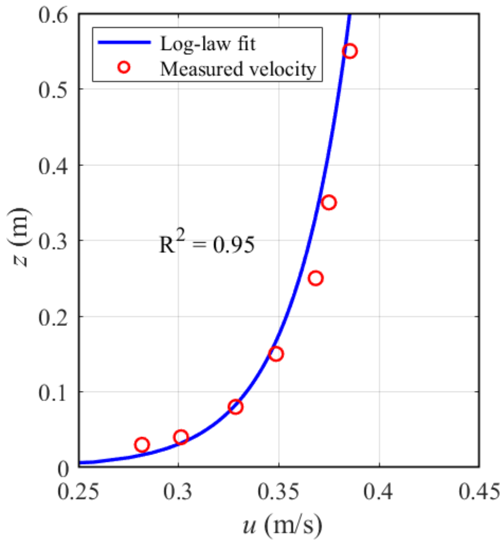

Fig. S6. Measured velocity data and logarithmic law fit lines

Section S5. Calculation of bed shear stress

During calm weather, the velocity structure of the bottom boundary layer is thought to exhibit a logarithmic velocity profile, which is taken to back-calculate the bed shear stresses under the action of the currents. The wall log-law (Smart, 2022) is expressed as follows:

$$u = \frac{u_\tau}{\kappa} \ln\left(\frac{z}{z_0}\right) \tag{S14}$$

where u_τ is the friction velocity, κ = 0.41 is the von Karman constant, $z_0 \approx 0.115\upsilon/u_\tau$ when hydraulically smooth condition, υ is kinematic viscosity of the fluid, d_{50} is the median grain size. During ESWS, u is obtained using the EMCM instrument, and during RDWS, u is obtained using the ADV.

Therefore, the bed shear stress induced by ocean currents is expressed as:

$$\tau_f = \rho_w u_\tau^2 \tag{S15}$$

where $\rho_w = 1025 \text{kg/m}^3$ is the density of seawater.

References

Aasland, T.E., Pettersen, B., Andersson, H.I. and Jiang, F., 2022. Revisiting the reattachment regime: a closer look at tandem cylinder flow at. J. Fluid Mech. 953.

Alemi, M., Pêgo, J.P. and Maia, R., 2019. Numerical simulation of the turbulent flow around a complex bridge pier on the scoured bed. Eur. J. Mech. B/Fluids. 76: 316-331.

Beheshti, A.A., Ataie-Ashtiani, B., 2008. Analysis of threshold and incipient conditions for sediment movement. Coast. Eng. 55, 423–430.

Dallali, M. and Armenio, V., 2015. Large eddy simulation of two-way coupling sediment transport. Adv. Water Resour. 81: 33-44.

Dey, S., Raju, U.V., 2002. Incipient Motion of Gravel and Coal Beds. Sadhana 27 (Part 5), 559 – 568 Part 5 (Printed in India).
Goring, D.G., Nikora, V.I., 2002. Despiking acoustic Doppler velocimeter data. J. Hydraul. Eng. 128 (1), 117–126.
Ong, M.C., Utnes, T., Holmedal, L.E., Myrhaug, D. and Pettersen, B., 2009. Numerical simulation of flow around a smooth circular cylinder at very high Reynolds numbers. Mar. Struct. 22(2): 142-153.
Singh, U.K., Jamei, M., Karbasi, M., Malik, A. and Pandey, M., 2022. Application of a modern multi-level ensemble approach for the estimation of critical shear stress in cohesive sediment mixture. J. Hydrol. 607: 127549.
Smart, G., 2022. A base for the log law and von Karman's constant problem. J. Hydraul. Res. 60(6): 935-943.
Z. Ruijin, River Sediment Dynamics, Ver. 2, China Water & Power Press, Beijing, China, 1998.